J Mater Sci (2009) 44:6754–6763
DOI 10.1007/s10853-009-3628-z

MESOSTRUCTURED MATERIALS

Phosphorus and nitrogen co-doped titania photocatalysts with a hierarchical meso-/macroporous structure

Gao-Song Shao · Tian-Yi Ma · Xue-Jun Zhang · Tie-Zhen Ren · Zhong-Yong Yuan

Received: 29 November 2008 / Accepted: 19 May 2009 / Published online: 9 June 2009

Abstract Visible light-active phosphorus and nitrogen co-doped meso-/macroporous titania materials were prepared by a simple two-step approach of the direct phosphation with the use of phosphoric acid solution and the succedent nitridation with the use of the urea solution. The prepared materials were characterized by UV–vis, solid-state ^{31}P MAS NMR, FT-IR, XPS, XRD, SEM, TEM, and N_2 adsorption analysis. Direct synthesis of phosphorus-doped meso-/macroporous titania materials could inhibit the formation of brookite phase and increase the surface area significantly, resulting in the hierarchical porous framework of nanocrystalline anatase phase with enhanced thermal stability and large porosity, and these features retained during the subsequent nitridation. The incorporation of P and N in the anatase titania lattice in the form of O–Ti–N, O–P–N, and Ti–O–P linkages was evidenced, and the extension of the absorption edges into the visible region and the corresponding narrowing of band gaps were observed in these N and P co-doped meso-/macroporous titanias, giving a higher photocatalytic activity in the degradation of Rhodamine B dye under visible-light irradiation than the samples doped with only N or P. The beneficial effect of hierarchical meso-/macroporous structure is also examined.

G.-S. Shao · T.-Y. Ma · X.-J. Zhang · Z.-Y. Yuan (✉)
Institute of New Catalytic Materials Science, Key Laboratory of Energy-Material Chemistry (Tianjin) & Engineering Research Center of Energy Storage and Conversion (Ministry of Education), College of Chemistry, Nankai University, Tianjin 300071, People's Republic of China
e-mail: zyyuan@nankai.edu.cn

T.-Z. Ren
School of Chemical Engineering and Technology, Hebei University of Technology, Tianjin 300130, People's Republic of China

Introduction

Visible-light photocatalysis has attracted intense interest because of its potential in utilization of solar energy recently [1–3]. Substitutional doping of TiO_2 with either anions (N, C, and S mostly) or cations has been found to be an effective method to achieve efficient photocatalysts in the visible-light range by reducing the band gap of titania [4–8]. The enhanced thermal stability and improved photocatalytic activity can also be exhibited in the phosphate-modified or phosphorus-doped titanias [9–12]. Yu et al. [9] found that direct incorporation of phosphorus from H_3PO_4 could stabilize the TiO_2 porous framework and increase the photocatalytic activity significantly. Körösi et al. [10] investigated systematically phosphate-modified titanias of varying phosphate contents. Shi et al. [11] and Lin et al. [12] demonstrated that the doping of phosphorus could efficiently inhibit the grain growth and enhance the surface area of TiO_2 nanoparticles, giving favorable photocatalytic property in the visible-light range. Further enhanced photocatalytic activity could be obtained in the phosphorus and nitrogen co-doped titania [13].

The further improving photocatalytic activity might be found in the nanocrystalline titania with mesoporous structure because of its abundant pores and large surface area, and several metal or nonmetal ion-doped titania mesoporous photocatalysts were reported [9, 14–21]. Furthermore, the incorporation of macropores in mesoporous materials, forming hierarchical pore structures at different length scales, could give enhanced properties due to

increased mass transport through the material and maintenance of a specific surface area on the level of fine pore systems [22, 23]. Since the macroporous channels could serve as light-transfer paths for the distribution of photon energy onto the large surface of inner photoactive mesoporous frameworks, hierarchical meso-/macroporous titania material has demonstrated to show the enhancement of photocatalytic activity due to the increasing photoabsorption efficiency and efficient diffusion of molecules caused by the macropores [24], though limited in the UV range. Our previous work also revealed that the substitutional N-doping of this meso-/macroporous titania material extended effectively its photocatalytic performance into the visible light region with increased activity [25].

In this work, we report the preparation of nitrogen and phosphorus co-doped titania materials with hierarchical meso-/macroporous structures by a simple two-step process, i.e., the direct phosphation of meso-/macroporous titania from phosphoric acid during the hydrolysis of titanium butoxide, and the followed nitridation with the use of urea. The hierarchical structure and the co-doping of phosphorus and nitrogen appear to have a cooperative effect on the synthesized photocatalysts, which show a narrower band gap than pure titania and the absorption tail in the visible range, and consequently is active in the photocatalytic oxidative decomposition of organic compound such as RhB under visible-light irradiation.

Experimental

Sample preparation

All chemicals were used as received, without further purification. Hierarchical meso-/macroporous phosphated titania was firstly synthesized by low-temperature hydrothermal treatment in the absence of surfactant. In a typical procedure, 8.7 g of tetrabutyl titanate (Kermel, AR) was dropwise added into 30 mL of phosphoric acid solution (pH = 1 or 2) under slow stirring at room temperature until the titanium *n*-alkoxide hydrolyzed completely. The mixture was transferred into a Teflon-lined autoclave and heated statically in an oven at 60 °C for 2 days. The product was then filtered, washed, and dried, which was used as precursor for further nitridation to fabricate the P and N co-doped titania materials.

Two grams of the above phosphated (P-doped) titania powder was mixed with 5 mL of urea aqueous solution (2 mol/L), and slowly magnetically stirred at room temperature for 5 h. The mixture was kept at room temperature for 48 h, and then washed with deionized water, and dried at 60 °C in air. Finally the obtained powders were calcined at 350, 400, or 450 °C for 2 h, and the samples were denoted as *x*PNT*y*, where *x* represents the pH value of phosphoric acid solution used, and *y* represents the calcination temperature. Correspondingly, only phosphorus-doped titania samples after calcination were denoted as *x*PT*y*. For comparison, meso-/macroporous pure titania was prepared in the absence of phosphoric acid [25], and its nitridation samples with the use of same 2 mol/L urea solution were denoted as NT*y*.

Sample characterization

X-ray diffraction (XRD) patterns were collected on a Rigaku D/max-2500 diffractometer with CuK_α radiation operated at 40 kV and 100 mA.

N_2 adsorption–desorption isotherms were recorded on a Quantachrome NOVA 2000e sorption analyzer at liquid nitrogen temperature (77 K). The samples were degassed at 200 °C overnight prior to the measurement. The surface area was obtained by the Brunauer–Emmett–Teller (BET) method, and pore size distribution was calculated from the adsorption branch of the isotherm by the Barret–Joyner–Halenda (BJH) model.

Scanning electron microscopy (SEM) was taken on a Shimadzu SS-550 microscope at 15 keV. Transmission electron microscopy (TEM) was carried out on a Philips Tecnai G20 microscope, working at 200 kV. A trace amount of sample was dispersed in ethanol solution by sonication for 10 min, and then deposited on a carbon-coated copper grid, which was used as a TEM specimen.

Fourier transform infrared (FT-IR) spectroscopy was carried out on a Bruker VECTOR 22 spectrometer, with KBr pellet technique.

UV–vis absorbance spectroscopy was employed on a JASCO V-570 UV-V-NIR spectrophotometer over the wavelength range 200–800 nm, using $BaSO_4$ as a reference.

X-ray photoelectron spectroscopy (XPS) measurements were performed on a Kratos Axis Ultra DLD (delay line detector) spectrometer equipped with a monochromatic Al-K_α X-ray source (1486.6 eV). All XPS spectra were recorded using an aperture slot of 300 × 700 μm, survey spectra were recorded with a pass energy of 160 eV, and high resolution spectra with a pass energy of 40 eV. The C1s peak of contamination (285.0 eV) was taken as an internal standard.

Solid-state ^{31}P magic-angle spinning (MAS) nuclear magnetic resonance (NMR) spectra were recorded on a Varian Infinityplus 400 MHz spectrometer operating at resonance frequency of 161.9 MHz and spinning rate of 12 kHz at room temperature, a 1.5 μs pulse with a repetition time of 5 s. Chemical shifts were indicated using an external H_3PO_4 reference (0 ppm).

Measurement of photocatalytic activity

The photocatalytic activity of the prepared catalysts was evaluated by the degradation of Rhodamine B (RhB) dye under visible-light irradiation. Twenty milligrams of the catalyst powder was placed into a tubular quartz reactor of 100 mL of RhB aqueous solution (1×10^{-5} mol/L, pH = 6), and a 40-watt tungsten bulb was used as the visible-light source, of which the wavelength range is usually considered as 400–2500 nm, located at 10 cm higher than the solution surrounded by a circulating water tube. All runs were conducted at ambient pressure and temperature. The suspensions were magnetically stirred in the dark for 30 min to ensure the establishment of an adsorption/desorption equilibrium, and then exposed to the light irradiation at room temperature. At given time intervals, about 5 mL of liquor was sampled, centrifuged for 5 min to discard any sediment. The absorbance of reaction solutions was measured using an SP-722 spectrometer at $\lambda_{max} = 554$ nm for RhB dye.

Results and discussion

Morphology, porosity, and crystal structure

The macrostructure of the synthesized materials were examined by scanning electron microscopy. Figure 1 shows the representative SEM images of the phosphorus and nitrogen co-doped titania materials synthesized without surfactant, revealing a uniform macroporous structure in different concentrations of phosphoric acid. The direct phosphated titanias, before nitridation, have the same macroporous structure (not shown), indicating that the macrostructure was retained during the thermal treatment of nitridation. The macropores are channel-like with the size in the range of 500–2000 nm and the length of 3–6 μm. The macrochannels are mainly of one-dimensional orientation, parallel to each other. Moreover, careful examination of the SEM micrographs reveals that the walls of the macropores are composed of small interconnected granular particles, leaving small holes in the macropore-walls of 200–600 nm in thickness. The TEM images (Fig. 1) of these materials also reveal that the macropore walls consist of the titania nanoparticles, and the worm-hole-like mesopores in the macroporous frameworks resulted from the nanoparticle assembly are observed.

Such a hierarchically meso-/macroporous structure is similar with those previously reported in the spontaneous template-free assembly of ordered macroporous titania, alumina, aluminosilicate, titanium and zirconium phosphates [26–31]. The hydrolysis of Ti-alkoxide precursors in phosphoric acid solution system results in the rapid formation of phosphated titania particles and the alcohol by-product, which might produce microphase-separated domains of titania-based nanoparticles and water/alcohol channels that are the initiators of the macrochannels. The following autoclaving will consolidate the regular self-assembly of the nanoparticles which could create a connected worm-like mesoporous channels. This meso-/macroporous structure is stable and can endure during the nitridation process.

The N_2 adsorption–desorption isotherms and the corresponding pore size distributions of the synthesized materials are shown in Fig. 2, and their textural properties are listed in Table 1. The isotherms correspond to Type IV adsorption isotherms with gradual increase at high P/P_0. Most of samples give a hysteresis loop of Type H3 due to the appearance of the capillary condensation, suggesting the existence of slit-shaped capillaries with parallel plates [32]. The BJH pore size distributions of the materials are calculated, giving asymmetric peaks in the range of 2–10 nm. This mesoporosity is probably partially due to the intraparticle porosity and partially due to the interparticle porosity, as confirmed by the SEM and TEM images of the fine particulate morphology. All these N and P co-doped titania samples possess very high BET surface areas of 206–247 m^2/g (Table 1), in comparison with the previous reported meso-/macroporous N-doped titania with the same urea concentration and the calcination temperature (121 m^2/g for NT450), though a little lower than that of P-doped titania sample (267 m^2/g for 1PT450). It is also seen from Table 1 that the surface areas of the *x*PNT*y* samples gradually decreased with the increase of either the nitridation temperature or the pH value of the phosphoric acid solution used. It is indicated that the direct phosphation (or P-doping) favor the formation of hierarchical materials with high surface areas and thermal stability.

X-ray diffraction was performed to investigate the structural phases and crystallite sizes of the samples. Figure 3 shows the XRD patterns of the prepared meso-/macroporous pure titania and N- and P-doped titania materials. The meso-/macroporous pure titania (T) and its nitridation product (NT450) presented bicrystalline phases of anatase and brookite [25], but the P-doped sample 1PT450 and N and P co-doped sample 1PNT450 exhibited only the anatase phase. This indicates that the direct P-doping could effectively inhibit the production of brookite phase. The effects of nitridation temperature on the crystal structures and particle sizes of the meso-/macroporous *x*PNT*y* samples are shown in Fig. 3 and Table 1. No other phases than anatase were observed, indicating that the presence of foreign ions does not cause disturbance of the overall anatase structure, though there is still a possibility of local distortions caused by incorporation of these foreign ions either at substitutional sites or at interstitial sites, and

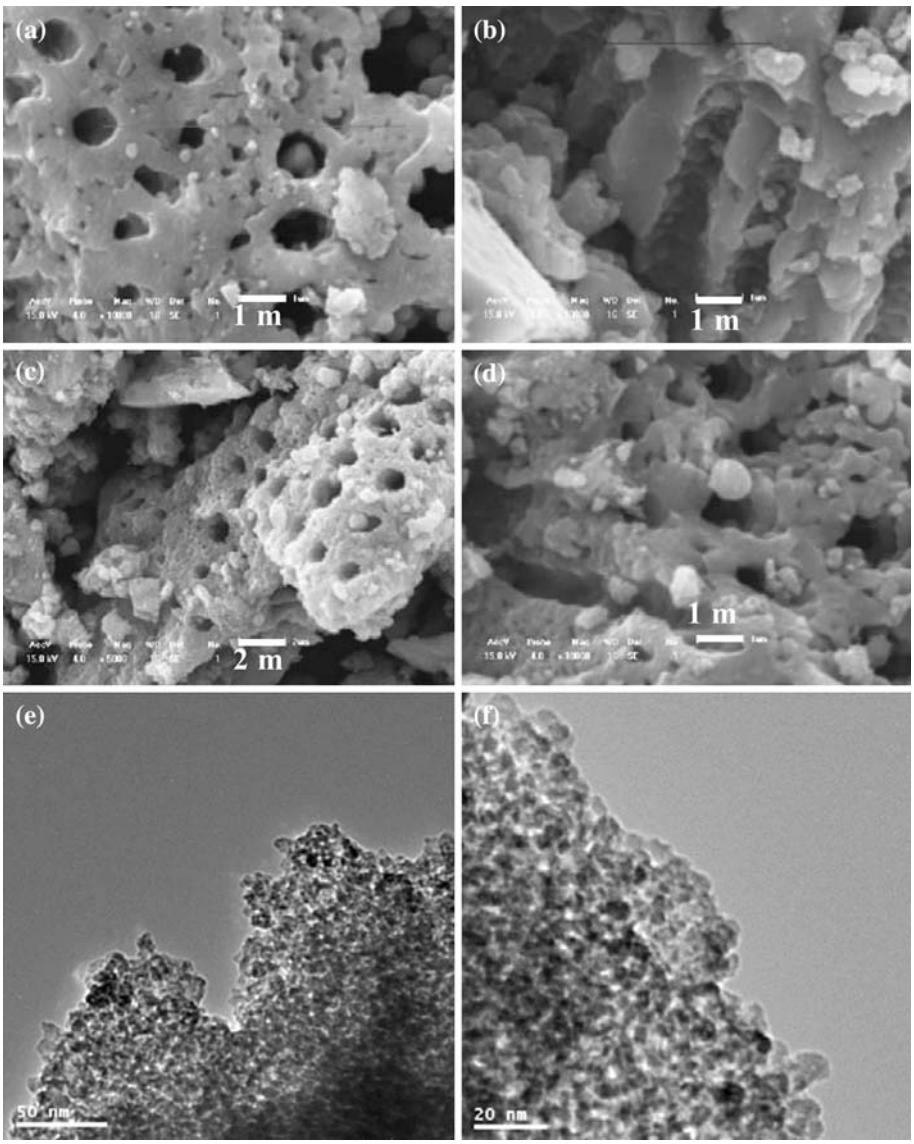

Fig. 1 SEM images of the prepared samples 1PNT450 (**a** and **b**) and 2PNT450 (**c** and **d**), and TEM images of samples 1PNT450 (**e**) and 2PNT450 (**f**)

also be attributed to the fact that the foreign species are present as a highly dispersed state in TiO_2 [33]. The intensity of the diffraction peaks increased with the nitridation temperature from 350 to 450 °C, suggesting the growth of the anatase nanoparticles with the increase of the calcination temperature. The particle sizes estimated by using the Scherrer formula [34], according to the anatase (101) peaks located at $2\theta = 25.2$–$25.3°$, are listed in Table 1. The average crystallite sizes of 1PNT*y* samples are smaller than those of 2PNT*y*. However, all *x*PNT*y* samples present the average crystallite sizes much smaller than the sample NT*y*, revealing the effects of P-doping on the crystal growth.

Chemical structure and composition

The FT-IR spectra of the samples NT450, 1PT450, 1PNT450, and 2PNT450 are shown in Fig. 4. Low-frequency bands in the range 466–566 cm^{-1} correspond to the Ti–O–Ti vibration of the network [15, 35]. The broad band at 3400 cm^{-1} and the band at 1630 cm^{-1} correspond to the surface-adsorbed water and hydroxyl groups. These bands in 1PNT450 and 2PNT450 are stronger than those in NT450 and 1PT450, indicating that modification of the N and P species increases the surface-adsorbed water and hydroxyl groups of titania, which may be significant for their photocatalytic activity, because the surface-adsorbed water and hydroxyl groups could act as photoexcited hole traps on the catalytic surface and produce hydroxyl radicals that are powerful oxidants in degrading organics [9, 36]. One additional shoulder band around 3180 cm^{-1} is present in 1PNT450 and 2PNT450, but not observable in NT450 and 1PT450. The samples 1PNT450 and 2PNT450 present one strong band at 1405 cm^{-1}, and sample NT450 presents one small band at 1391 cm^{-1}, while for the sample

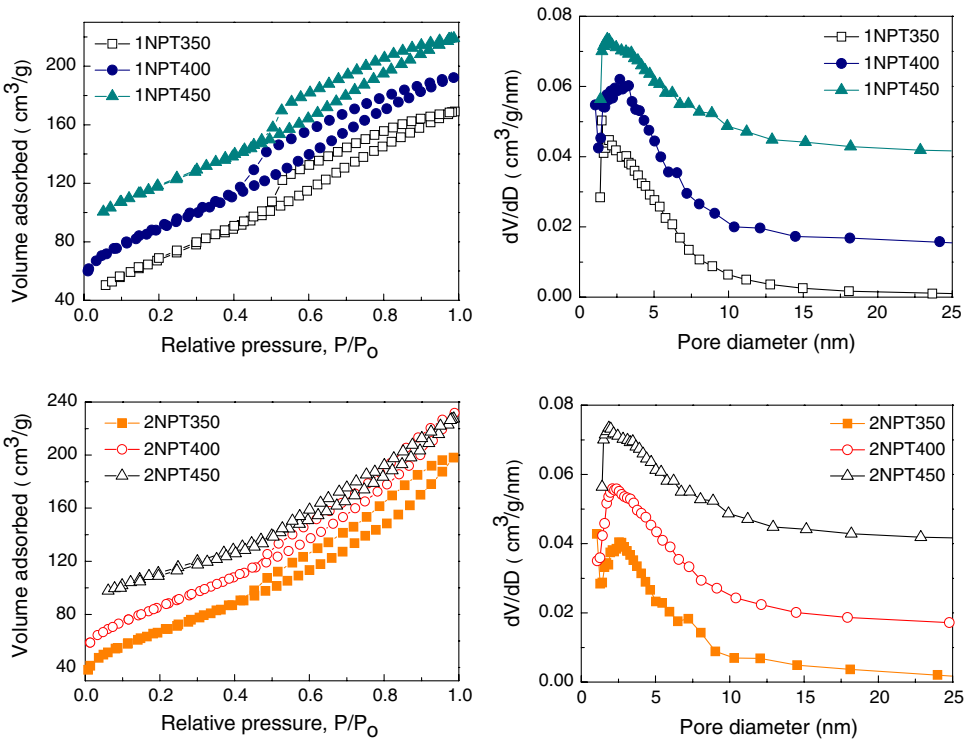

Fig. 2 (*left*) N_2 adsorption–desorption isotherms and (*right*) the corresponding BJH pore size distribution curves of the prepared samples. The volume adsorbed was shifted by 20 and 55 and the d*V*/d*D* value was shifted by 0.015 and 0.04 for the curves of dataset samples heated 400 and 450, respectively

Table 1 Summary of the physicochemical properties of the prepared samples

Samples	Anatase crystallite size[a] (nm)	S_{BET}[b] (m^2/g)	$D_{BJH\text{-}ads}$[c] (nm)	D_{ave}[d] (nm)	V_{pore}[e] (cm^3/g)	Band gap(eV)	
						E_{g1}	E_{g2}
1PNT350	4.3	248	2.1	4.2	0.26	3.21	2.5
1PNT400	5.3	247	2.9	4.3	0.27	3.28	2.48
1PNT450	7.1	231	3.2	4.4	0.25	3.25	2.54
2PNT350	4.5	239	2.8	5.1	0.31	3.23	2.55
2PNT400	7.1	238	2.3	4.3	0.27	3.19	2.37
2PNT450	7.2	206	3.3	5.2	0.27	3.26	2.47
1PT450	6.2	267	1.9	4.1	0.28	3.22	2.5
NT450	14.8	121	5.4	5.2	0.16	3.09	2.48

[a] Calculated by the Scherrer formula

[b] BET surface area calculated from the linear part of the BET plot

[c] Estimated using the adsorption branch of the isotherm by the BJH method

[d] Average pore size

[e] Single point total pore volume of pores at $P/P_0 = 0.98$

1PT450, the band in this frequency is too weak to be identified. Furthermore, an adsorption peak at 1051–1033 cm^{-1} is observed in the FT-IR spectra of P-doped samples (*x*PT*y* and *x*PNT*y*) but is absence in the samples NT450 and pure titania. The band at 1051–1033 cm^{-1} is often characteristic of PO_4^{3-} [37, 38] and recently is somewhat regarded as the contribution of Ti–O–P bond [36, 38]. The bands at 1390–1406 cm^{-1} can be attributed to either the phosphoryl (P=O) groups in PO_4^{3-} or the vibrational mode of hyponitrite or the superposition of these two signals. Relative to the little band at 1390 cm^{-1} in the spectrum of NT450, the bands corresponding to the N species are shifted to 1405 cm^{-1} for *x*PNT*y*, which should be the effect of doped P on N species. A small band at 1125 cm^{-1} in the spectrum of NT450, corresponding to the N species, is not observed in the *x*PNT*y*, which may be hidden by the P–O bending vibration of PO_4^{3-} groups in *x*PNT*y*. Therefore, it is deduced that the phosphorus exists not only in the form of PO_4^{3-}, but also probably in the form of Ti–O–P, and the nitrogen atoms are embedded in

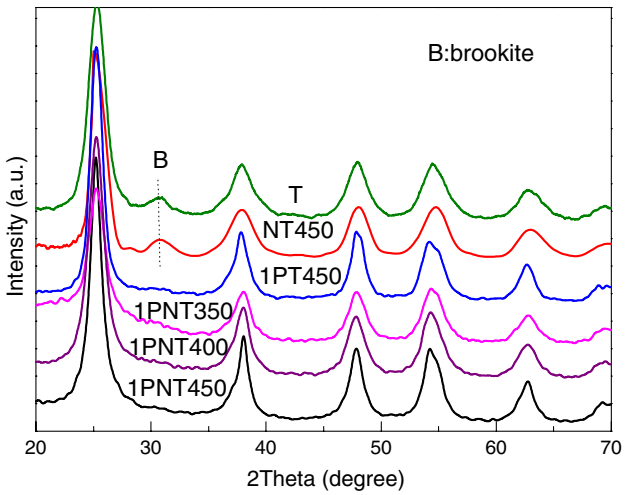

Fig. 3 XRD patterns of the prepared meso-/macroporous pure titania (T) and N- and P-doped titania samples

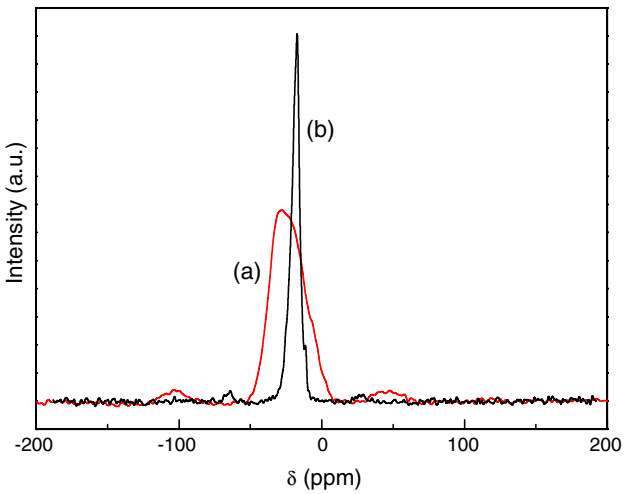

Fig. 5 ^{31}P MAS NMR spectra of the samples (*a*) 1PNT450 and (*b*) 2PNT450

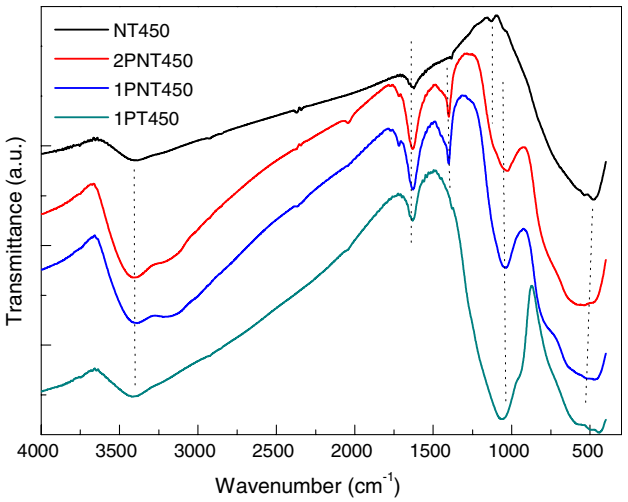

Fig. 4 The FT-IR spectra of the prepared samples

the TiO_2 network by replacing the oxygen atom in the formation of the O–Ti–N. The shoulder bands around 3180 cm^{-1} observed in 1PNT450 and 2PNT450 may be attributed to the effect of doped N on P species, in the form N–Ti–P or O–P–N bonds.

^{31}P MAS NMR spectroscopy was employed to study the phosphorus microenvironments (Fig. 5). The sample 1PNT450 shows a broad signal at the chemical shifts of approximately −27 ppm, which can be assigned tetrahedral phosphorus environments connected with four O–Ti bands [$P(OTi)_4$] [31, 38]. The broadening of the ^{31}P NMR stems from the wide distribution of phosphorus among sites with slightly different environments. However, the sample 2PNT450 gives one intense peak at −3 ppm, which is in good agreement with chemical shift values for phosphorus coordinated via oxygen to half or one titanium atoms [31, 38], i.e., $P(OTi)_x(OH)_{4-x}$, where $x = 1$ or 0.5. Since the samples 1PNT450 and 2PNT450 were prepared by the nitridation of the precursor direct-phosphated in H_3PO_4 solution of pH = 1 and 2, respectively, the concentration of H_3PO_4 solution affected seriously the chemical microenvironments of phosphorus, let alone the textural properties and thermal stability aforementioned. According to the peak area, the phosphorus content in the sample 1PNT450 is about 1.3-fold than in 2PNT450.

Figure 6 shows the XPS survey spectra and high-resolution spectra of N1s, Ti2p, P2p, and O1s, taken on the surface of the NT450, 1PNT450, and 2PTN450 samples. Figure 6b shows the XPS spectra of the samples in the $Ti2p_{1/2}$ and $Ti2p_{3/2}$ binding energy (BE) regions. The $Ti2p_{3/2}$ peak is centered at 458.3, 458.7, and 458.6 eV, and the $Ti2p_{1/2}$ peak at 464.1, 464.4, and 464.3 eV for the NT450, 1PNT450, and 2PNT450 samples, respectively. These binding energies are characteristic of Ti^{4+} [39] and the peak position of Ti^{4+} is significantly influenced by its coordination environment. Compared with the binding energy of pure TiO_2 (459 eV for $Ti2p_{3/2}$ and 464.8 eV for $Ti2p_{1/2}$) [31], the binding energies of Ti2p in the phosphorus and nitrogen co-doped samples (2PNT450 and 1PNT450) are lower than those of pure TiO_2, but are slightly higher than only nitrogen-doped titania (NT450). This is the result from different electronic interactions of Ti with anions, which causes partial electron transformation from the N and P to the Ti and an increase of the electron density on Ti because of the lower electronegativity of nitrogen and phosphor compared to oxygen (O > N > P) [40]. The O1s signals of NT450, 1PNT450, and 2PNT450 samples are shown in Fig. 6c. In comparison with the almost symmetric O1s spectrum of pure TiO_2 at the binding energy of 530.2 eV, the O1s spectra of P- or/and N-co-doped titanias are clearly asymmetric, having a

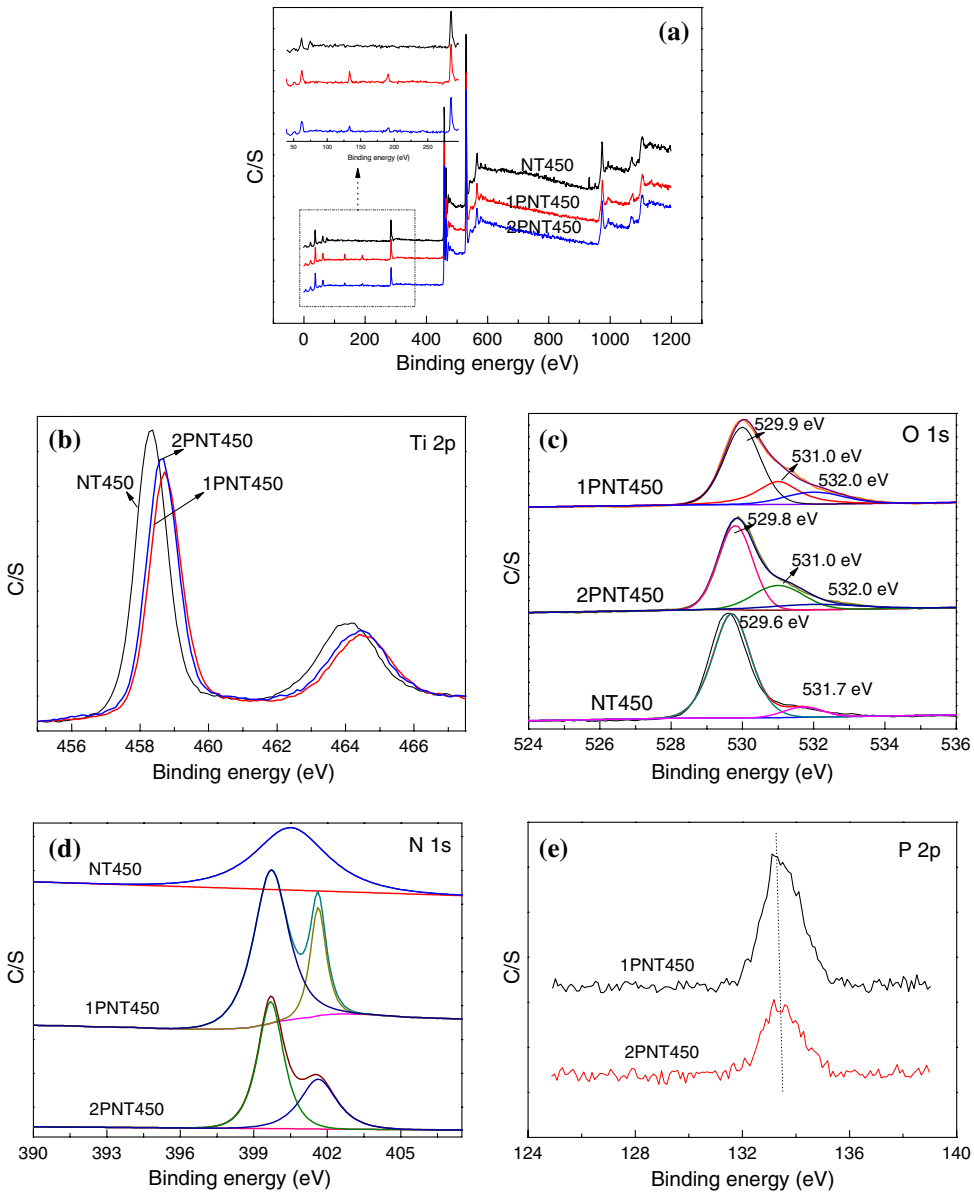

Fig. 6 XPS spectra of the samples. **a** Survey, **b** Ti2P, **c** O1s, **d** N1s, **e** P2p

low-intensity shoulder on the high binding energy side, which can be fitted by two to three peaks. The main peaks of NT450, 1PNT450, and 2PNT450 samples situated at 529.6, 529.9, and 529.8 eV, respectively, corresponding to the oxygen in Ti–O bonds [10, 31], which are a little lower than that of pure TiO_2. The shift order of the main O1s energy position is the same as that of the Ti2p energy position, suggesting the successful incorporation of nitrogen and phosphorus into the TiO_2 lattice to form the O–Ti–N and Ti–O–P bonds, respectively. The obvious shoulder peaks at 531.0 eV in the O1s spectra of 1PNT450 and 2PNT450 could be ascribed to oxygen in the P–O bonds [9, 10, 31], which was absent in the sample NT450. The small peaks at round 531.7–532.0 eV could be assigned to the hydroxyl groups [10, 31].

The N1s spectrum (Fig. 6d) of NT450 exhibits only one peak at 400.4 eV. While both the samples 1PNT450 and 2PNT450 give two peaks at 399.7 and 401.6 eV. The binding energies of these peaks are higher than that of TiN appeared at $\leq$397.5 eV [41], and lower than that of hyponitrite type nitrogen at 404 eV. The main peak of 399–402 eV might be attributed to the anionic N^- in O–Ti–N linkages, though this line was attributed to adsorbed molecular nitrogen in some literature [42, 43]. The observed N1s peak splitting in 1PNT450 and 2PNT450 confirms the effect of N- and P-co-doping. The overlapped peaks at 401.6 and 399.7 eV could be ascribed to the nitrogen atom-substituted oxygen in the crystalline TiO_2 lattice to form the O–Ti–N structure and the nitrogen species coordinated to P in the form of O–P–N linkage [13], respectively.

To get further evidence, the P states are also examined by XPS spectra. As seen from Fig. 6a, the spectra of the samples 1PNT450 and 2PNT450 in the binding energy range of 130–190 eV are different from that of the sample NT450. The high-resolution XPS P2p spectra (Fig. 6e) of the 1PNT450 and 2PNT450 samples show single peak at 133.5 and 133.4 eV, respectively, suggesting that P ions are in the pentavalent-oxidation state (P^{5+}) [44]. It is unlikely that Ti–P bonds are present in our P-doped meso-/macroporous TiO_2, since the characteristic peak of P2p in TiP at 128.6 eV was not observed [45]. Thus, it is expected that the P^{5+} might replace a part of Ti^{4+} in the crystal lattice of TiO_2 to form the bond P–O–Ti [13], similar to S^{6+}- [21, 46, 47] and I^{5+}- [17] doped TiO_2, but not simple phosphate (or PO_4^{3-}), which resulted in the charge imbalance and the decrease of the recombination rate of photogenerated electrons and holes. However, the nature of interaction between P and TiO_2 is not quite clear currently, which remains a problem worthy of further study.

As mentioned above, N and P atoms are probably incorporated as anions and cations, replacing O and Ti ions partly in the anatase titania lattice, respectively. The binding energies of N1s confirm N species exist in the form of the O–Ti–N and/or O–P–N bonds. The binding energies of P2p confirm P exists in the form of the P–O–Ti and/or N–P–O bonds [13]. A shift of Ti2p and O1s toward lower binding energy upon nitridation further demonstrates the successful incorporation of nitrogen into the TiO_2 lattice. The surface atomic compositions of NT450, 2PNT450, and 1PNT450 determined by the XPS results are listed in Table 2. The bulky atomic ratio of P/Ti (obtained by ICP) is lower than the surface atomic P/Ti ratio, indicating that most of the detected N and P species are in the surface layers of the meso-/macroporous titanias.

Optical property and photocatalytic activity

The UV–vis absorbance spectra of the prepared *x*PNT*y* samples are shown in Fig. 7. The absorption is at $\sim$ <400 nm for pure TiO_2 (not shown), while the yellow colored phosphorus and nitrogen co-doped meso-/macroporous titanias exhibit the absorption edge extending into the visible region, >400 nm. Obviously, the *x*PNT*y* samples show a high tailing absorbance in the visible range, giving two absorption edges. The band gap energies (E_g) can be calculated by the formula $E_g = 1239.8/\lambda_g$ from the wavelength values corresponding to the intersection point of the vertical and horizontal parts of the spectra (λ_g) [48], and the corresponding band gaps (E_{g1} and E_{g2}) are listed in Table 1. The absorption edges at 377.7–388.0 nm (E_{g1}: 3.28–3.2 eV) and 488.4–520.0 nm (E_{g2}: 2.54–2.38 eV) are observed in the *x*PNT*y* samples. The first edges are related to the band structure of the original titania, and the second ones correspond to the newly formed N2p and P2p bands that are located above the O2p valence band. However, although the decrease of the band gaps of *x*PNT*y* samples is obvious in comparison with the meso-/macroporous pure TiO_2 (band gap of 3.18 eV), the band gaps of NT450 is still comparable with those of 1PNT450 and 2PNT450. The narrowing of band gaps of the prepared N and P co-doped meso-/macroporous titanias might be resulted from the interaction of titania with phosphorus and nitrogen in lower oxidation state, suggesting that they should be possibly responsive to the visible light.

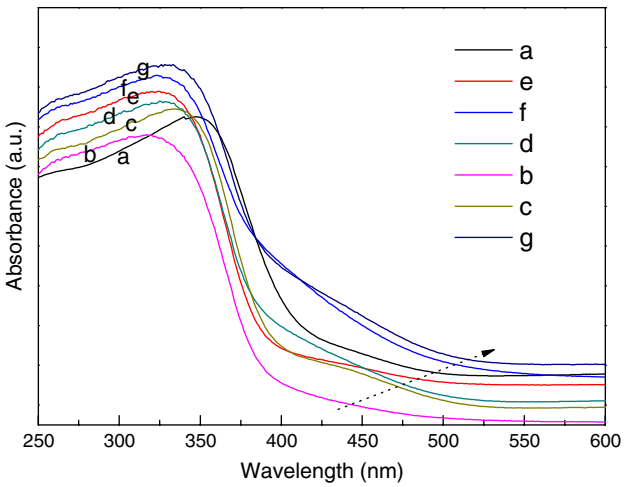

Fig 7 The UV–vis absorbance spectra of (*a*) NT450, (*b*) 2PNT350, (*c*) 2PNT400, (*d*) 2PNT450, (*e*) 1PNT350, (*f*) 1PNT400, (*g*) 1PNT450

Table 2 Atomic compositions determined by the XPS and ICP

Samples	Mass content by XPS (%)				Mass content by ICP (%)	
	N	P	Ti	O	Ti	P
NT450	1.43	0	55.81	42.76	–	–
2PNT450	0.59	3.39	51.63	44.40	35.94	1.32
1PNT450	0.88	5.37	47.88	45.87	–	–

The photocatalytic activities of the obtained meso-/macroporous phosphorus and nitrogen co-doped TiO_2 were tested by the degradation of RhB under visible-light irradiation (Fig. 8). For comparison, a blank experiment (self-photosensitized process, in the absence of any catalysts), P25, meso-/macroporous pure TiO_2 (T), and only phosphorus or nitrogen-doped meso-/macroporous titania catalysts were performed under identical conditions. The RhB degradation efficiency is increased with the visible-light irradiation time. It is seen from Fig. 8 that the self-degradation process under visible-light irradiation is inactive, as evidenced by only 1.1% of RhB degraded after 80 min irradiation. The commercial non-porous P25 and the

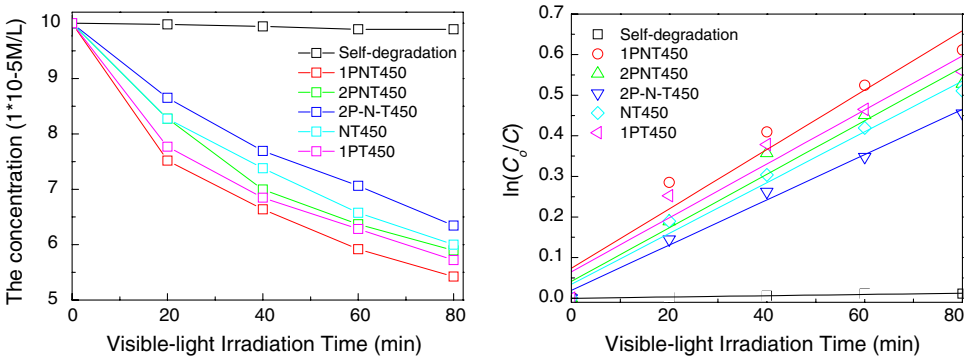

Fig. 8 (*left*) The residual concentration of RhB solution under visible-light irradiation by the prepared catalysts; (*right*) a plot of $\ln(C_o/C)$ versus the irradiation time, showing the fitting results using the pseudo-first-order reaction

meso-/macroporous pure titania [25] have 11.2 and 30.4% of RhB degraded after 80 min irradiation, respectively, indicating the effect of meso-/macroporous structure with high surface area due to light penetrating and molecular diffusing [25]. However, 40, 42.78, and 45.75% of RhB were degraded for NT450, 1PT450, and 1PNT450 after 80 min irradiation, respectively, demonstrating the superior performance of the N- and/or P-doped meso-/macroporous titania samples. The photocatalytic activity of 1PNT450 is better than that of both NT450 and 1PT450, which may be the result of the co-doping of N and P in the meso-/macroporous titania, suggesting the possible cooperation effect of doped N and P species. As to the photocatalyst 2NPT450, 41.04% of RhB was degraded after 80 min irradiation, indicating its lower photocatalytic activity than 1NPT450, which is related to the lower contents of P and N in 2NPT450 than in 1NPT450.

To further substantiate the beneficial effects of macrochannels in the materials, we destroyed the macrochannels of 2PNT450 by milling, and the resulted catalyst was denoted as 2P-N-T450, which still possessed mesoporous structure but the macroporous structure was destroyed. As shown in Fig 8, there was a 5.4% drop (from 41.0 to 35.6%) in photocatalytic activity after destruction of macrochannels. It is thus confirmed the significance of hierarchically meso-/macroporous structure of the *x*PNT*y* materials in improving photocatalytic activity, since the macroporous channels could serve as light-transfer paths for the distribution of photon energy onto the large surface of inner photoactive mesoporous frameworks, and allow rapid diffusion of various reactants and products during photocatalytic reaction process, and the mesoporous structure of high surface area can offer more active sites (hydroxyl groups) for photocatalytic reaction.

The relationship between $\ln(C_0/C)$ and the irradiation time t for the visible-light degradation of RhB is also shown in Fig. 8. By plotting $\ln(C_0/C)$ as a function of irradiation time through regression, we obtained for each catalyst sample the pseudo-first-order reaction rate constant k (min^{-1}) from the slopes of the simulated straight lines. The self-degradation rate constant of RhB is 1.6×10^{-4}, while the degradation rate constants of RhB for catalysts 1PNT450, 2PNT450, 1PT450, NT450, and 2P-N-T450 are 7.3×10^{-3}, 6.5×10^{-3}, 6.6×10^{-3}, 6.3×10^{-3}, and 5.5×10^{-3}, respectively. The photocatalytic results clearly indicate that the meso-/macropores structure and the co-doping with N and P can effectively favor the improved photocatalytic activity in the visible-light region.

Conclusions

Meso-/macroporous P and N co-doped titania materials with high surface area have been prepared by a two-step process of direct phosphation and followed nitridation, which possess anatase phase of nanocrystalline structure. It has been demonstrated that the incorporation of phosphorus and nitrogen in meso-/macroporous TiO_2 materials can efficiently inhibit the grain growth and phase transformation, increase the surface area, and improve the thermal stability. The features of hierarchical meso-/macroporous structure with nano-anatase TiO_2 in the framework and N and P co-doping make the new material a highly effective photocatalyst in visible-light degradation of RhB, since the intradiffusion resistance is minimized and the efficiency of photoabsorption is enhanced. These TiO_2-based materials with hierarchal pore network, strong light-harvesting capability, and easy surface modification, may also be promising as an advanced catalytic support and novel optic/electric material.

Acknowledgements This work was supported by the National Natural Science Foundation of China (20473041, 20673060), the National Basic Research Program of China (2009CB623502), the Specialized Research Fund for the Doctoral Program of Higher Education (20070055014), the Natural Science Foundation of Tianjin (08JCZDJC21500), the Chinese-Bulgarian Scientific and Technological Cooperation Project, the Fund from Hebei Provincial Department of Education (2007313), the Program for New Century Excellent Talents in University (NCET-06-0215), and Nankai University.

References

1. Chatti R, Rayalu SS, Dubey N, Labhsetwar N, Devotta S (2007) Sol Energy Mater Sol Cells 91:180
2. Asahi R, Morikawa T, Ohwaki T, Aoki K, Tage Y (2001) Science 293:269
3. Kasahara A, Nukumizu K, Hitoki G, Takata T, Kondo JN, Hara M, Kobayashi H, Domen K (2002) J Phys Chem A 106:6750
4. Sakthivel S, Janczarek M, Kisch H (2004) J Phys Chem B 108:19384
5. Ohno T, Miyamoto Z, Nishijima K, Kanemitsu H, Feng X (2006) Appl Catal A Gen 302:62
6. Nakano Y, Morikawa T, Ohwaki T, Taga Y (2006) Physica B 376–377:823
7. Ghicov A, Schmidt B, Kunze J, Schmuki P (2007) Chem Phys Lett 433:323
8. Shen M, Wu Z, Huang H, Du Y, Yang P (2006) Mater Lett 60:693
9. Yu JC, Zhang L, Zheng Z, Zhao J (2003) Chem Mater 15:2280
10. Körösi L, Papp S, Bertóti I, Dékány I (2007) Chem Mater 19:4811
11. Shi Q, Yang D, Jiang Z, Li J (2006) J Mol Catal B Enzym 43:44
12. Lin L, Lin W, Xie JL, Zhu YX, Zhao BY, Xie YC (2007) Appl Catal B Environ 75:52
13. Lin L, Zheng RY, Xie JL, Zhu YX, Xie YC (2007) Appl Catal B Environ 76:196
14. Luo H, Wang C, Yan Y (2003) Chem Mater 15:3841
15. Peng T, Zhao D, Dai K, Shi W, Hirao K (2005) J Phys Chem B 109:4947
16. Sheng Q, Cong Y, Yuan S, Zhang J, Anpo M (2006) Microporous Mesoporous Mater 95:220
17. Hong XT, Wang ZP, Cai WM, Lu F, Zhang J, Yang YZ, Ma N, Liu YJ (2005) Chem Mater 17:1548
18. Chen C, Li X, Ma W, Zhao J, Hidaka H, Serpone N (2002) J Phys Chem B 106:318
19. Sakthivel S, Kisch H (2003) ChemPhysChem 4:487
20. Yu JC, Zhang L, Yu J (2002) Chem Mater 14:4647
21. Yu JC, Ho W, Yu JG, Yip H, Wong PK, Zhao JC (2005) Environ Sci Technol 39:1175
22. Yu J, Zhang L, Cheng B, Su Y (2007) J Phys Chem C 111:10582
23. Yuan ZY, Su BL (2006) J Mater Chem 16:663
24. Wang X, Yu JC, Ho C, Hou Y, Fu X (2005) Langmuir 21:2552
25. Shao G-S, Zhang X-J, Yuan Z-Y (2008) Appl Catal B Environ 82:208
26. Collins A, Carriazo D, Davis SA, Mann S (2004) Chem Commun 568–569
27. Ren TZ, Yuan ZY, Su SL (2004) Chem Commun 2730–2731
28. Deng W, Shanks BH (2005) Chem Mater 17:3092
29. Leonard A, Su BL (2004) Chem Commun 14:1674
30. Yuan ZY, Ren TZ, Azioune A, Pireaux JJ, Su BL (2006) Chem Mater 18:1753
31. Ren TZ, Yuan ZY, Azioune A, Pireaux JJ, Su BL (2006) Langmuir 22:3886
32. Kruk M, Jaroniec M (2001) Chem Mater 13:3169
33. Xu YH, Chen HR, Zeng ZX, Lei B (2006) Appl Surf Sci 252:8565
34. Klug HP, Alexander LE (1974) X-ray diffraction procedure for polycrystalline and amorphous materials, 2nd edn. Wiley, New York
35. Soler-Illia GJAA, Louis A, Sanchez C (2002) Chem Mater 14:750
36. Ding Z, Lu GQ, Greenfield PF (2000) J Phys Chem B 104:4815
37. Samantaray SK, Parida K (2001) Appl Catal A Gen 220:9
38. Bhaumik A, Inagaki S (2001) J Am Chem Soc 123:691
39. Ramqvist L, Hamrin K, Johansson G, Fahlmann A, Nordling C (1969) J Phys Chem Solids 30:1835
40. Cong Y, Zhang J, Chen F, Anpo M (2007) J Phys Chem C 111:6976
41. Saha NC, Tompkins HG (1992) J Appl Phys 72:3072
42. György E, Pérez del Pino A, Serra P, Morenza JL (2003) Surf Coat Technol 173:265
43. Battiston GA, Gerbasi R, Gregori A, Porchia M, Cattarin S, Rizzi GA (2000) Thin Solid Films 371:126
44. Splinter SJ, Rofagha R, Mcintyre NS, Erb U (1996) Surf Interface Anal 24:181
45. Baunack S, Oswald S, Scharnweber D (1998) Surf Interface Anal 26:471
46. Ohno T, Mitsui T, Matsumura M (2003) Chem Lett 32:364
47. Ohno T, Akiyoshi M, Umebayashi T, Asai K, Mitsui T, Matsumura M (2004) Appl Catal A 265:115
48. Kõrösi L, Dékány I (2006) Colloids Surf A 280:146